

Chapter 2

Antenna/RF Design and Analog Self-Interference Cancellation



Jong Woo Kwak, Min Soo Sim, In-Woong Kang, Jaedon Park,
and Chan-Byoung Chae

Abstract The main obstacle to full-duplex radios is self-interference (SI). To overcome SI, researchers have proposed several analog and digital domain self-interference cancellation (SIC) techniques. Digital cancellation has the following limitations: (1) It is only possible if the SI is sufficiently removed in the analog domain to fall within the dynamic range of an analog-to-digital converter (ADC). (2) It cannot mitigate the transmitter noise. Thus, analog cancellation plays an important role in a SIC scenario. This chapter provides an overview of current research activities on the analog cancellation scheme. Analog cancellation can be categorized into two classes—passive and active. In the passive analog cancellation, an RF component suppresses the SI. This can be implemented using a circulator or antenna separation. Leakages are cancelled by the active analog cancellation, which is based on a channel estimation of residual SI channel. The leakage from the passive cancellation can be matched by a signal generated from a tunable circuit or an auxiliary transmit chain. A key issue then in active analog cancellation is designing a circuit and optimization algorithm.

2.1 Introduction

In the demand of increasing spectral efficiency and data rates, full-duplex has emerged as a highly promising technique for 5G wireless communications. Full-duplex radio has the potential to double the spectral efficiency by transmitting and receiving simultaneously on the same frequency. The main challenge in the full-duplex radio is self-interference (SI)—a phenomenon where a transmit signal is received by its own receiver. Without the self-interference cancellation (SIC),

J. W. Kwak · M. S. Sim · C.-B. Chae (✉)
Yonsei University, Seoul, Korea
e-mail: kjw8216@yonsei.ac.kr; simms@yonsei.ac.kr; cbchae@yonsei.ac.kr

I.-W. Kang · J. Park
Agency for Defense Development, Daejeon, Korea
e-mail: iwkang@add.re.kr; jaedon2@add.re.kr

the SI significantly degrades the signal-of-interest. To alleviate this problem, the traditional wireless communication systems operate in half-duplex which separates the uplink and downlink transmission in either time domain (TDD) or frequency domain (FDD).

Recently, many SIC methods have been proposed. SIC can be categorized, roughly, into two classes: (1) intrinsic cancellation and (2) SI channel estimation-based cancellation. In the intrinsic cancellation, the SI is weakened in a passive manner using antenna separation, antenna cancellation, or an isolator. The intrinsic cancellation is often called passive analog cancellation since it is done in the analog domain. The remaining SI from passive analog cancellation is mitigated by the SI channel estimation-based cancellation. Since the TX signal is known perfectly, the SI can be reconstructed through SI channel estimation. The reconstructed SI is then subtracted from the received signal leaving the signal-of-interest. Conventional channel estimation methods can be easily applied for the SIC in the baseband. The greatest hurdle in the SIC is the fact that ADC has to convert the SI and signal-of-interest simultaneously. To avoid ADC saturation, an additional cancellation is adopted in the analog domain; this is called active analog cancellation. The active analog cancellation regenerates the destructive SI in the analog domain. It is also based on the SI channel estimation which is done in the digital domain.

Because the SI channel estimation in the digital cancellation is dependent on the result of the analog cancellation, the analog cancellation plays a crucial role in the SIC. The realm of analog cancellation research covers the designing of the antenna/RF components and digital signal processing. The size of analog canceller, power/computational costs must be designed so as to be implementable. Another hurdle is the limited bandwidth of the RF component. Recently, researchers have proposed a photonics-based analog cancellation system to provide a broadband cancellation.

This chapter provides an overview of the state-of-the-art analog cancellation methods. The rest of this chapter is organized as follows: In Sect. 2.2, the main obstacles in full-duplex system are introduced. Section 2.3 presents the passive cancellation methods and Sect. 2.4 presents the analog cancellation methods. In Sect. 2.5, a numerical analysis of the SIC is provided through simulation. The digital cancellation method is briefly introduced in Sect. 2.5.

2.2 Requirements for a Full-Duplex System

To carry out full-duplex communication, SI must be suppressed at the receiver thermal noise floor. In a multiple-antenna system, the passive analog cancellation can be achieved by using a directive antenna or an antenna cancellation technique. If the transmitter and the receiver share the single antenna, an isolator is required to separate the SI.

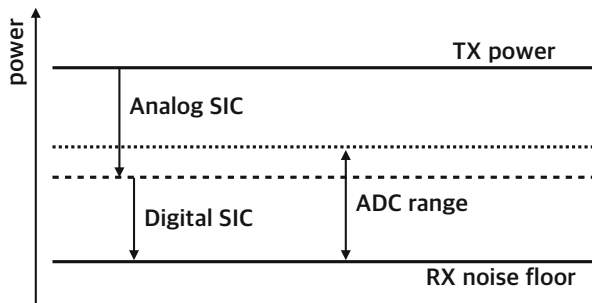
The remaining SI from passive analog cancellation consists of linear components and nonlinear components. Linear components are caused by multi-path propagation between transmitter and receiver. In the single-antenna system with a circulator, leakages from the circulator are modeled as linear. Nonlinear components mainly come from power amplifier nonlinearity, ADC quantization noise, transmitter noise, and other RF imperfections.

The channel estimation-based cancellation can be made in both the analog and digital domains. This cancellation involves three steps. (1) Construct a model of the SI channel. (2) Estimate the SI channel using perfect knowledge of transmit signal. (3) Reconstruct and subtract the SI from the received signal. Linear components of SI can be easily mitigated by the existing channel estimation methods. The power amplifier nonlinearity and I/Q imbalance are modeled in [8, 9]. The main obstacle of SIC is a required ADC dynamic range to acquire the SI and signal-of-interest simultaneously. A dynamic range of a q -bit ADC is calculated as

$$6.02 \times q + 1.76 \text{ [dB]}. \quad (2.1)$$

In the case of the 14-bit ADC, the dynamic range is 86 dB. This means that the SI power after analog cancellation should not be higher than the receiver noise floor by 86 dB. Figure 2.1 depicts an example of the power levels in the successful SIC scenario. Essentially, the ADC dynamic range determines a required analog cancellation amount. Typically, it is not possible to achieve this with the intrinsic cancellation alone. Hence, most of the full-duplex systems adopt an additional active cancellation in the analog domain, which is also based on the SI channel estimation. Figure 2.2 shows a full-duplex system adopting a combination of analog and digital domain SIC.

Fig. 2.1 An example of the power levels in the successful SIC scenario



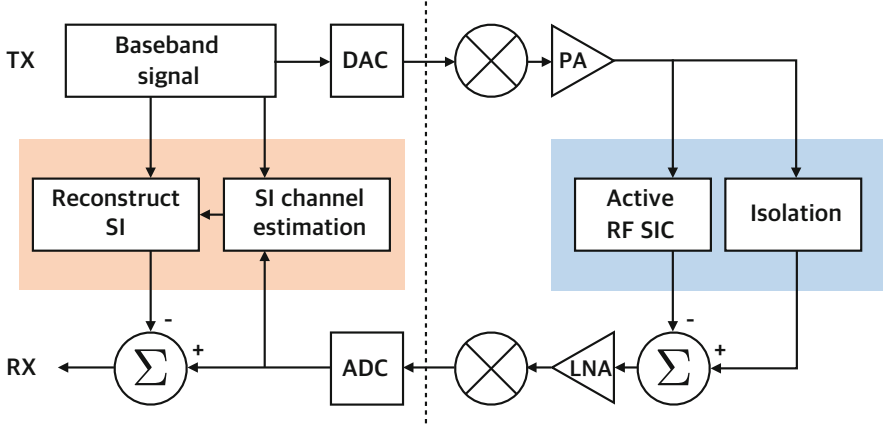


Fig. 2.2 A block diagram of a full-duplex system with SIC

2.3 Passive Analog Cancellation

In the propagation stage, an isolator separates the desired signal and the SI. An active RF component is not needed here. Therefore, it is often called passive analog cancellation. The most intuitive way is to separate the antenna for the transmit chain and the receive chain. The path loss between two antennas can be described as

$$L = 10n \log 10d + C, \quad (2.2)$$

where L , n , d , and C denote the path loss, the path loss exponent, the distance between two antennas, and a system-dependent constant, respectively. As (2.2) shows, the cancellation amount determined by a size of the transceiver.

Another solution is antenna cancellation, which generates a π -phase rotated SI signal at the receiver. Figure 2.3 describes an asymmetric antenna cancellation setup. The wavelength of the transmit signal is denoted as λ . The distance between TX1 and RX (d_1) is $\lambda/2$ larger than the distance between Tx2 and Rx (d_2). At RX, the two transmit signals will have a phase difference of π . To compensate for the different path loss, we have to allocate more power to the TX2. Ideally, the SI will be perfectly mitigated whereas the additional transmit signal acts as interference for the other receiver. The authors in [3] combined the interference cancellation methods for the antenna cancellation. The asymmetric antenna cancellation method is inherently available in the narrow bandwidth (due to λ).

To alleviate the bandwidth dependency, a symmetric antenna cancellation method is adopted in [4]. Figure 2.4 depicts a symmetric antenna cancellation. A π -phase shifter is employed instead of having a difference in the distance. The passive cancellation methods using polarized antenna are presented in [5, 6]. In [6], a dual-polarized antenna is implemented in a real-time full-duplex LTE prototype.

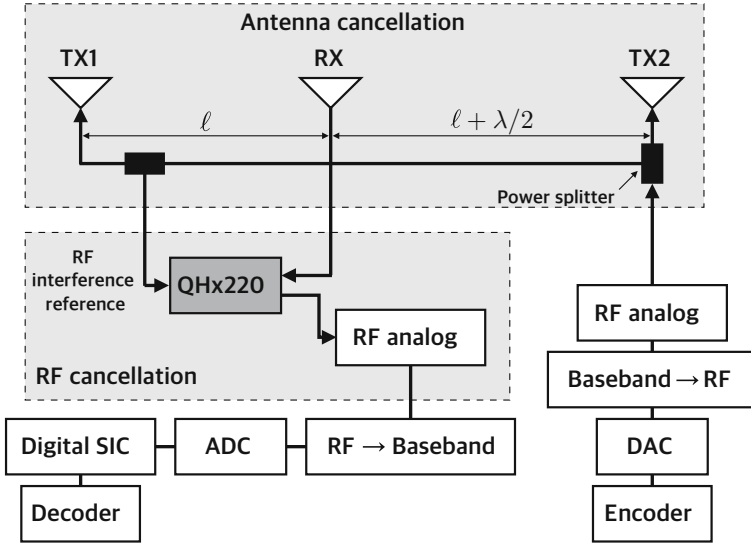


Fig. 2.3 System architecture proposed in [3]

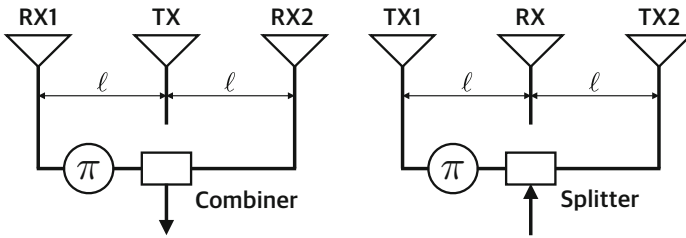


Fig. 2.4 Symmetric antenna cancellation using a π -phase shifter [4]

In single-antenna full-duplex radios, to achieve a passive cancellation, one needs a circulator. A circulator is a 3-port device that steers the signal entering any port is transmitted to the next port only. Ferrite circulators are often used in the communication systems. When a signal enters to port 1, the ferrite changes a magnetic resonance pattern to create a null at port 3. The circulator can provide isolation in a narrow bandwidth. Figure 2.5 shows the SI components in the circulator setup.

The strongest SI component is direct leakage. Typically, a circulator provides 20–30 dB isolation for the direct leakage. The remaining SI components are mitigated by an active analog cancellation. The second component is the signal reflected by an antenna. The reflected power (return loss) can be computed as

$$L_{\text{ret}} = -20 \log \left| \frac{Z_L - Z_S}{Z_L + Z_S} \right|, \quad (2.3)$$

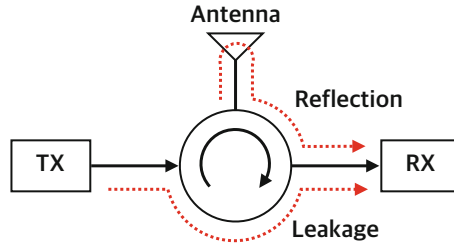


Fig. 2.5 Remaining SI components in the circulator setup

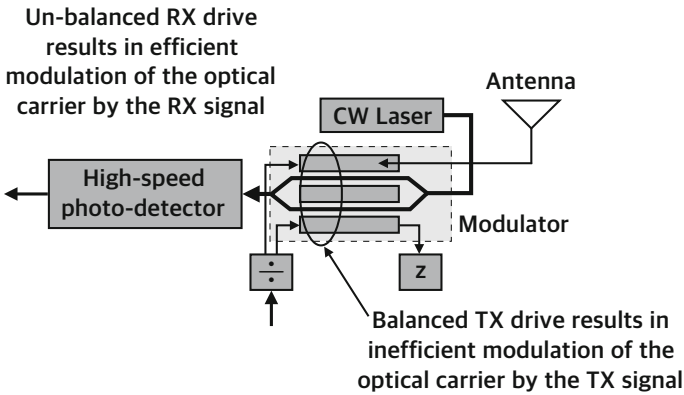


Fig. 2.6 A block diagram of the optical circulator proposed in [10]

where Z_L is a load impedance and Z_S is a source impedance. The power of the third component is an environmental-reflected signal that depends on the objects near the transceiver.

An optical circulator is proposed by a company called Photonic Systems Incorporated [10]. This optical circulator achieves better isolation and bandwidth dependency compared to the conventional RF circulator. Figure 2.6 depicts a block diagram of the optical circulator.

The received signal from the antenna is fed to a balanced optical modulator, whereas the transmit signal is just conveyed as an electrical signal. Since the transmit signal propagates in the opposite direction to the optical carrier, the modulation—the response of the transmit signal—is extremely low. The effect of the transmit signal reflected by the antenna—which propagates in the same direction as the optical carrier—can be compensated by a balance port. A principle of the optical modulator is in [2]. An experimental result of the optical circulator prototype is provided in [11]. Roughly, the optical circulator achieves 30–40 dB isolation from 2.5–20 GHz.

A fundamental limitation of passive analog cancellation is that it cannot suppress the SI reflected from the environment. The authors in [20] compare the remaining SI after passive cancellation in an anechoic chamber and a highly reflective room with

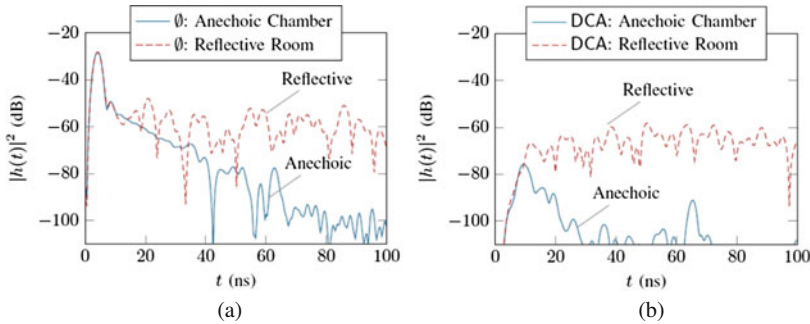


Fig. 2.7 Comparison between the time responses measured in an anechoic chamber and a reflective room. © [2014] IEEE. Reprinted, with permission, from ref. [20]. (a) No passive analog cancellation. (b) Directionals, Crosspol, Absorber (DCA)

metal walls (Fig. 2.7). Combinations of directional isolation, absorptive shielding (i.e., place an RF-absorptive material between transceivers to increase the pathloss), and cross polarization are applied for the comparison. For the absorptive shielding, Eccosorb AN-79 is used as an absorber which consists of discrete layers of lossy material. An impedance of the incident layer of Eccosorb AN-79 is designed to be close to air. The impedance gradually increases from the incident layer to the rear layer. This graded multilayer structure offers broadband electromagnetic wave absorption capability compared to the single layer structure [20]. Figure 2.7a shows the time responses of the SI channel without SI cancellation. The initial part of the time response corresponds to the direct path and the tail corresponds to the reflective paths. As Figure 2.7b shows that passive analog cancellation only suppresses the direct path, and the remaining SI from the reflective paths can be severe in the reflective environment.

2.4 Active Analog Cancellation

2.4.1 Adaptive RF Circuits

The basic concept of the active analog cancellation is to generate a signal that matches to the leakage from passive analog cancellation. The signal can be generated using a tunable circuit and auxiliary transmit chain. In the tunable circuit-based active analog cancellation, a small copy of transmitted signal is fed to the circuit. Figure 2.8 shows a general multi-tap canceller consisting of M delay(τ_i) lines.

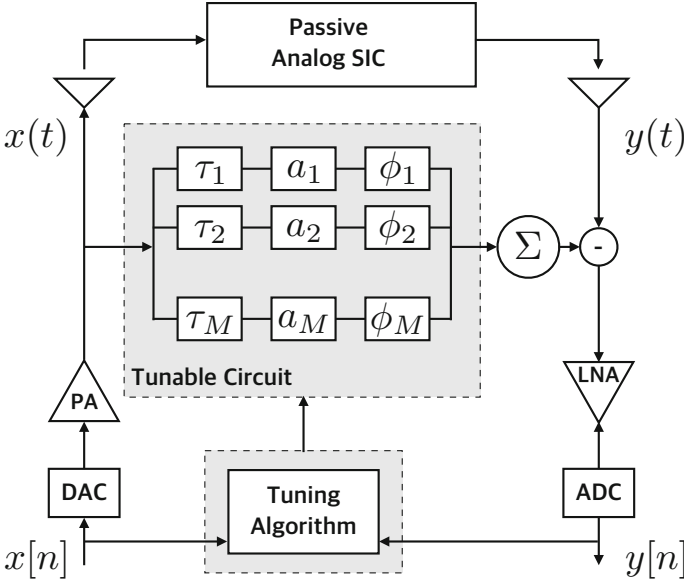


Fig. 2.8 A general design of an adaptive circuit for the active analog cancellation

Each delay line comprises an attenuator (a_i) and a phase shifter (ϕ_i). The parameters of the circuit are tuned via solving an optimization problem,

$$\min_{\tau, a, \phi} \left(y(t) - \sum_{i=1}^M x_{\tau_i, a_i, \phi_i}(t) \right)^2, \quad (2.4)$$

where $x_{\tau_i, a_i, \phi_i}(t)$ is an output signal of the each delay line, $y(t)$ is the leakage, $x(t)$ is the transmit signal. The optimization is performed in the digital domain (i.e., the optimization algorithm receives as input variables the baseband signal ($x[n]$, $y[n]$)). Note that the aim of analog cancellation is to avoid the ADC saturation. Therefore, at the initial stage, the SI signal is transmitted at weak power to carry out optimization while avoiding ADC saturation. After the parameters are tuned, full-duplex transmission is performed.

The authors in [13] proposed a novel optimization algorithm and architecture of adaptive circuit. The authors implemented the full-duplex WiFi radio in SISO scenario. Figure 2.9 shows the proposed full-duplex communication system. A circulator is used as a passive isolator. As discussed in Section (circulator), the leakage of the circulator consists of two primary components (i.e., direct leakage and reflected signal). Accordingly, an adaptive circuit should be designed to be suitable to cancel those two primary leakages.

The key idea is to fix the delays of the circuit using the characteristics of the leakage. Each delay line contains a variable attenuator. Theoretically, we can

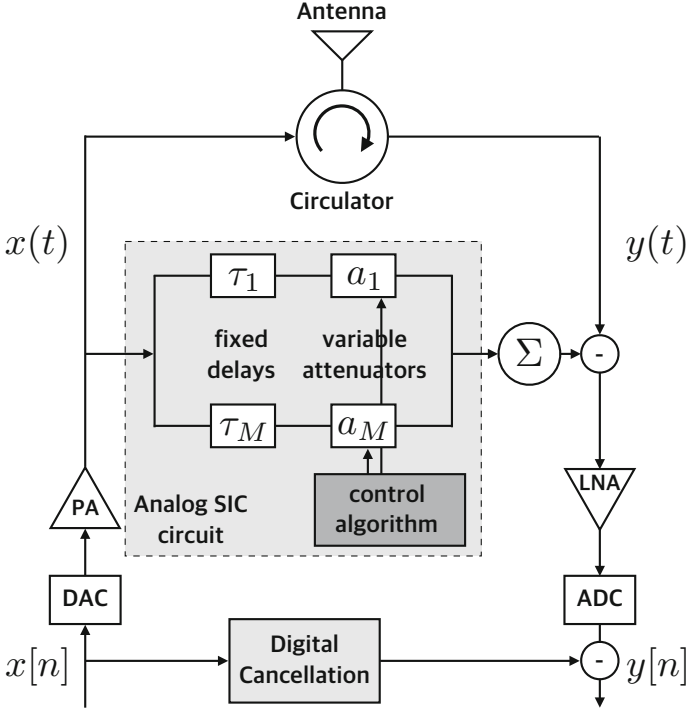


Fig. 2.9 System architecture proposed in [13]

regenerate the actual SI with appropriately chosen fixed delays even though the actual SI has an arbitrary delay within a certain range. Since the proposed method uses fixed delays, it does not require hard-to-implement high-resolution delays.

Let the actual SI ($y(t)$) have a delay d , an attenuating value a , and a Nyquist rate f_s . Assume that we set the delays (d_i) and attenuating values (a_i) of the circuit as (2.5),

$$d_i = d_{i-1} + \frac{1}{f_s}, \quad (2.5)$$

$$a_i = \text{sinc}(f_s(d - d_i)),$$

where $\text{sinc}(\cdot)$ is a sinc function (Fig. 2.10). This virtual circuit consists of infinitely many delay lines. Then the summation of the each delay line's output at time instant t_1 is

$$\sum_{i=-\infty}^{\infty} a_i x(t_1 - d_i) = \sum_{i=-\infty}^{\infty} \text{sinc}(f_s(d - d_i)) x(t_1 - d_i), \quad (2.6)$$

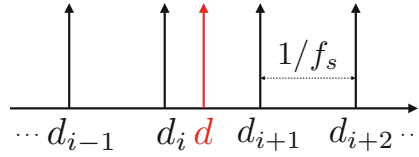


Fig. 2.10 An arrangement of the fixed delay

where actual SI at time instant t_1 is

$$y(t_1) = x(t_1 - d). \tag{2.7}$$

Since $x(t)$ is a band-limited signal, we can apply the Nyquist-sampling theorem and easily show that (2.6) is equal to (2.7). In other words, if we know the actual delay d with an infinite number of delay lines, the circuit can perfectly reconstruct the SI. Since the actual delay d is not known, an optimization algorithm adjusts the attenuator values to cancel the leakage.

To implement this algorithm in practice, there are some hurdles.

1. We have to configure the adaptive circuit with finite delay lines. It is obvious that the cancellation amount will increase as the number of delay lines increases. To make the full-duplex system implementable on mobile devices, however, it is preferable that the size of an adaptive circuit prefer to be small. The authors in [13] proposed a 16-tap (delay lines) 10×10 cm circuit. Figure 2.11 depicts the alignment of the fixed delays, where d_{dir} and d_{ref} denote the actual delays of the two primary leakages. To cancel the primary leakage $y_{\text{dir}}(t)$, the 8 equidistant delays are chosen over the actual delay d_{dir} . The authors in [13] investigated the variation range of the actual delay. They then picked the four delays below that range and the four delays above that range. Other delays are picked in the same way for the $y_{\text{ref}}(t)$ (i.e., reflection from the antenna).
2. A periodic optimization for the adaptive circuit causes a time overhead. The overhead depends heavily on the design of an optimization algorithm. A main

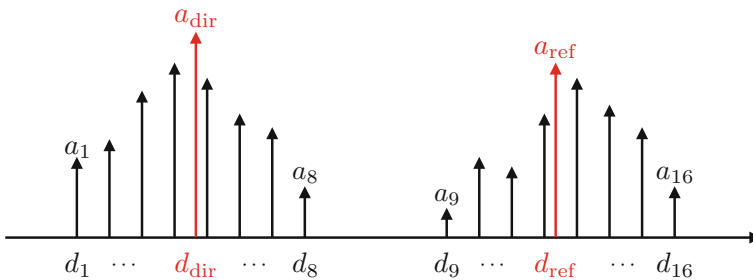


Fig. 2.11 An alignment of the fixed delays in [13]

challenge in the adaptive circuit-based analog cancellation is to reduce the time consumption for the optimization.

3. The variable components of the circuit have a finite resolution. The attenuator characteristics determine a feasible set of the optimization problem.

Given these limitations, the authors in [13] proposed a frequency response-based optimization algorithm. The basic concept of this algorithm is to represent the distortion ($H(f)$) introduced by the passive analog cancellation in the frequency domain as (2.11).

$$Y(f) = H(f)X(f), \quad (2.8)$$

where $Y(f)$ and $X(f)$ are the frequency domain representation of the leakage ($y(t)$) and tapped signal ($x(t)$), respectively. The frequency response $H(f)$ (i.e., an FFT the SI channel) can be measured using pilot symbols. After measuring $H(f)$, the circuit is tuned by solving

$$\min_{a_1, \dots, a_N} \left(H(f) - \sum_{i=1}^N H_i^{a_i}(f) \right)^2, \quad (2.9)$$

where $H^{a_i}(f)$ is the frequency response for delay line i for attenuation setting of a_i . The problem is two-fold. First, the $H_i^{a_i}(f)$ should be measured for every possible attenuation value a_i . Since the circuit is well connected, it is impossible to emulate the delay line individually to measure $H_i^{a_i}(f)$. To isolate the target delay line as much as possible, the authors set the highest attenuator values for all of the delay lines except the target one. The frequency response with another attenuation values can be computed using this initial measurement and a S-parameter data of the attenuator, which provide the relative change of the frequency response with the changing attenuation value. Second, we have to find an optimal attenuation setting to match the actual frequency response $H^{a_i}(f)$. If the attenuator can take 128 different values, there are 128^{16} possible cases in total. In this situation, an exhaustive search is not feasible. Therefore, the authors relaxed it to a linear program and then random rounding to get a feasible solution. The authors achieved 45–50 dB analog cancellation using their testbeds. The design above is extended to full-duplex MIMO system [14]. To achieve full-duplex MIMO, interference from a neighboring transmitter (i.e., cross talk) has to be mitigated. We can simply replicate the SISO design, as shown in Fig. 2.12.

The SISO replication-based design requires M^2 times more taps than the SISO design, where M is the number of transmit antenna. Hence, the computational complexity with respect to M increases exponentially. The authors in [14] proposed a cascaded cancellation design based on the following insight: since the antennas are close to one another, the crosstalk and self-talk will experience similar channels. The relationship between two channels can be modeled as

$$H_{ct}(f) = H_c(f)H_s(f), \quad (2.10)$$

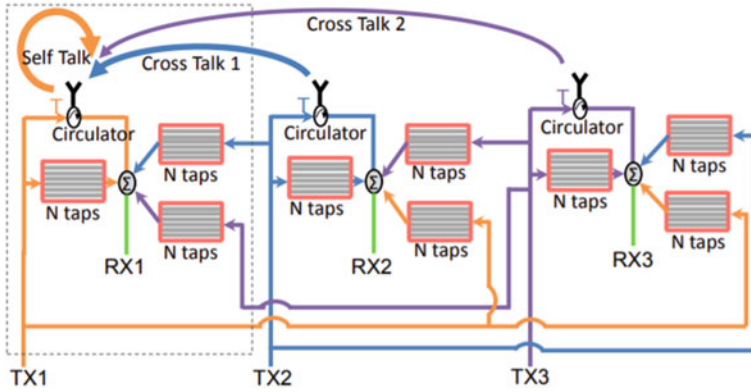


Fig. 2.12 SISO replication design proposed in [14]. Self-talk corresponds to the SI and cross talk corresponds to the interference from the neighbor transmitter

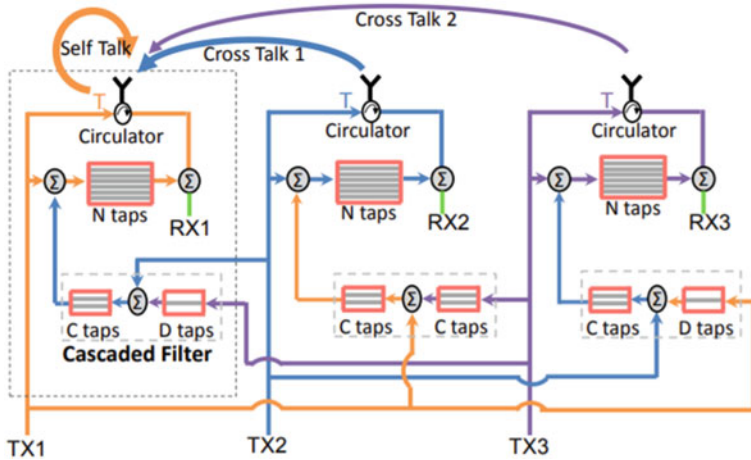


Fig. 2.13 Cascaded design proposed in [14]

where $H_{ct}(f)$ is a frequency response of the crosstalk channel, $H_s(f)$ is a frequency response of the self-talk channel, and $H_c(f)$ is a simple cascade transfer function.

Figure 2.13 illustrates a cascade cancellation design ($M = 3$). For the cascade transfer function of crosstalk channel 1 and 2, the adaptive circuit consists of C and D taps, respectively. Since the cascade transfer function is simple, we allocate the number of taps relatively small compared to N (i.e., $N \gg C > D$). The number of taps for cascade transfer functions (C, D) is empirically chosen to provide sufficient cancellation. The authors in [14] compared the SISO replication-based design and cascade cancellation design for a 3×3 MIMO full-duplex radio operating a WiFi PHY in a 20 MHz band at 0 dBm TX power. Figure 2.14 depicts a comparison of the two designs with the same number of taps. The results show that the cascade design is more efficient than the SISO replication-based design.

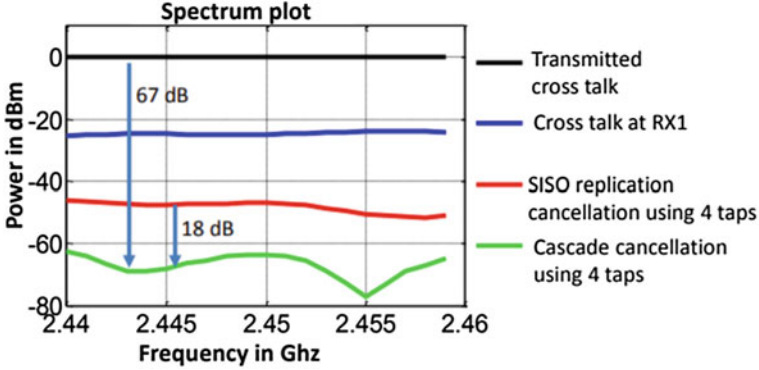


Fig. 2.14 Comparison of the SISO replication design and the cascaded design [14]

One of the other state-of-the-art analog cancellation technique is proposed in [7]. An adaptive circuit comprises fixed delay lines with variable phase shifters and attenuators in [7]. The main idea is to formulate the optimization problem as a convex problem. Consider an OFDM system with K subcarriers. Denote the sampling rate as $1/T_S$. The k -th frequency component of the adaptive circuit frequency response is modeled as

$$\mathbf{H}_{\text{cir}}[k] = \sum_{n=1}^N a_n e^{j\phi_n} e^{jk\delta_w \tau_n} = \Phi_k^T \mathbf{W} \quad (2.11)$$

where a_n , ϕ_n , τ_n , and δ_w are attenuation, phase shift, fixed delay of n -th path, and sampling interval over the bandwidth of interest, respectively. Note that the previous active cancellation method uses measured frequency response of delay line ($H^{a_i}(f)$). On the other hand, the authors in [7] theoretically modeled the frequency response of the adaptive circuit, enabling the analysis of residual SI power. The sampling interval $\delta_w = 2\pi B/K$, where B is the bandwidth of the $x(t)$. For convenience, we define the following two vectors:

$$\begin{aligned} \Phi_k &= \left[e^{-jw\delta_w k \tau_1}, e^{-jw\delta_w k \tau_2}, \dots, e^{-jw\delta_w k \tau_N} \right]^T, \\ \mathbf{W} &= \left[a_1 e^{-j\phi_1}, a_2 e^{-j\phi_2}, \dots, a_N e^{-j\phi_N} \right]. \end{aligned} \quad (2.12)$$

With a given fixed delay alignment ($\tau_1, \tau_2, \dots, \tau_N$), the optimization algorithm minimizes the difference between two sampled frequency response that can be formulated as

$$\min_w \mathbb{E} \left[\left(\mathbf{H}_{\text{chan}}[k] - \Phi_k^T \mathbf{W} \right) \left(\mathbf{H}_{\text{chan}}[k] - \Phi_k^T \mathbf{W} \right)^H \right], \quad (2.13)$$

where \mathbf{H}_{chan} and $(\cdot)^H$ denote the measured frequency response of the SI channel and Hermitian operation, respectively. Conceding that $\mathbf{H}_{\text{chan}}[k]$ and $\boldsymbol{\Phi}_k$ are jointly stationary, the object function is convex. Therefore, the global optimum ($\hat{\mathbf{W}}$) can be analytically obtained as

$$\begin{aligned}\hat{\mathbf{W}} &= \mathbb{E} \left[\overline{\boldsymbol{\Phi}_k \boldsymbol{\Phi}_k^T} \right]^{-1} \mathbb{E} \left[\mathbf{H}_{\text{chan}}[k] \overline{\boldsymbol{\Phi}_k} \right], \\ &= \mathbf{R}^{-1} \mathbf{P}\end{aligned}\quad (2.14)$$

where \mathbf{R} is a complex correlation matrix operating on a set of sampled complex exponentials and \mathbf{P} is a complex cross-correlation matrix operating on the measured channel response and set of complex exponentials. Note that \mathbf{R}^{-1} can be precomputed. The main advantage of this algorithm is that we can relieve the matrix inversion operation. The time complexity of this algorithm depends on the calculation of \mathbf{P} and the multiplication of \mathbf{R}^{-1} and \mathbf{P} .

In [18], the author analyzed the residual SI power after cancellation for the case of a time-invariant SI channel and a time-variant SI channel. For each case the authors considered the CSI imperfection and an imperfect delay alignment. The baseband equivalent time domain SI channel can be described as a uniformly spaced TDL model,

$$h_{\text{SI}}^b(t) = \sum_{i=0}^{\infty} h_i \left(t - \frac{i}{B} \right), \quad (2.15)$$

where h_i is the i -th tap coefficient. The authors in [18] set the fixed delays of an adaptive circuit as $(0, \frac{1}{B}, \dots, \frac{N-1}{B})$, where N is the number of delay lines. The estimated channel ($\hat{\mathbf{H}}(k)$) is modeled as

$$\hat{\mathbf{H}}[k] = \mathbf{H}[k] + \tilde{\mathbf{N}}[k], \quad (2.16)$$

where $\tilde{\mathbf{N}}[k]$ is the circularly symmetric complex Gaussian (CSCG) noise with zero mean and variance $\tilde{\sigma}^2$. The reconstructed frequency response of the circuit is $\hat{\mathbf{H}}_{\text{cir}} = [\boldsymbol{\Phi}_1^T \hat{\mathbf{W}}, \dots, \boldsymbol{\Phi}_K^T \hat{\mathbf{W}}]^T$. Then the average power of the residual (ρ_{rd}) is represented as

$$\begin{aligned}\rho_{rd} &= \frac{1}{K} \mathbb{E} \left\{ \left| \mathbf{X} \left(\mathbf{H} - \hat{\mathbf{H}}_{\text{cir}} \right) \right|^2 \right\} \\ &= \frac{1}{K} \mathbb{E} \left\{ \text{tr} \left[\left(\mathbf{H} - \hat{\mathbf{H}}_{\text{cir}} \right) \left(\mathbf{H} - \hat{\mathbf{H}}_{\text{cir}} \right)^H \mathbf{X}^H \mathbf{X} \right] \right\} \\ &= \frac{1}{K} \text{tr} \left\{ \mathbb{E} \left[\left(\mathbf{H} - \hat{\mathbf{H}}_{\text{cir}} \right) \left(\mathbf{H} - \hat{\mathbf{H}}_{\text{cir}} \right)^H \right] \right\},\end{aligned}\quad (2.17)$$

Table 2.1 Residual SI power on the time-varying channel for the 3 cases

Cases	Description	Power of Residual SI
Case 1	<ul style="list-style-type: none"> • Perfect SI channel CSI and perfect delay alignment • Time-varying SI channel with processing delay t_d 	$2 - \frac{2}{K_f+1} \{K_f + J_0[2\pi \Delta T f_d K T_S]\}$
Case 2	<ul style="list-style-type: none"> • Imperfect SI channel CSI and perfect delay alignment • Time-varying SI channel with processing delay t_d 	$\frac{N}{K} \tilde{\sigma}^2 + 2 - \frac{2}{K_f+1} \{K_f + J_0[2\pi \Delta T f_d K T_S]\}$
Case 3	<ul style="list-style-type: none"> • Imperfect SI channel CSI and imperfect delay alignment with $N = K$ and $\Delta t = 1/B$ • Time-varying SI channel with processing delay t_d • Time-varying SI channel with processing delay t_d 	$\tilde{\sigma}^2 + 2 - \frac{2}{K_f+1} \{K_f + J_0[2\pi \Delta T f_d K T_S]\}$

where $\mathbf{X} = \text{diag}\{\mathbf{X}(0), \mathbf{X}(1), \dots, \mathbf{X}(K)\}$ with $\mathbb{E}[|\mathbf{X}(k)|^2] = 1$ and $\mathbb{E}[|\mathbf{X}(k_1)\mathbf{X}(k_2)^*|^2] = 0, k_1 \neq k_2$, $\text{tr}(\cdot)$ denotes the trace of a matrix. With the notation $\Omega = [\Phi_1^T, \dots, \Phi_K^T]^T$ the authors in [18] derived the following,

$$\rho_{rd} = \frac{N}{K} \tilde{\sigma}^2 + \frac{N}{K} \text{tr}(\mathbf{H}\mathbf{H}^H - K\Omega\mathbf{R}\Omega^H\mathbf{H}\mathbf{H}^H). \quad (2.18)$$

The first term results from the imperfect SI CSI, while the second term results from the imperfect delay alignment.

Over the time-varying SI channel, the processing delay (i.e., time consumed in calculating the variable and tuning) comes up as an issue. In [18], the authors assume the processing delay t_d to be a multiple of the $K T_S$ (i.e., $t_d = \Delta T K T_S$, ΔT is an integer). In this case, the power of residual SI is analyzed in Table 2.1 [18].

2.4.2 Micro Photonic Canceller

To achieve broadband cancellation, researchers have proposed several micro-photonic cancellers (MPC). Similar to the RF adaptive circuit, the SI channel is reconstructed using tunable delays and attenuators. Essentially, the delay comes from changing the propagating group velocity using carrier dynamics. A set of optical time delay lines (OTDL) and optical variable attenuators is used in [12] to reconstruct the SI channel. This system achieves 40 dB cancellation over 50 MHz bandwidth. However, tuning the OTDL takes a great deal of time. To obtain a low-latency tunable delay, the authors in [16] used a semiconductor optical

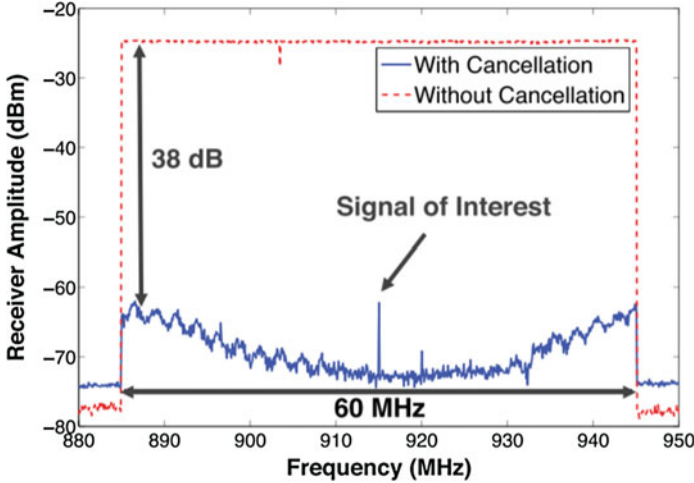


Fig. 2.15 Broadband cancellation result of the optical system. © [2016] IEEE. Reprinted, with permission, from ref. [16]

amplifier (SOA), which has 200 ns latency. The proposed system has a single SOA. Therefore, to tune the SOA involves a simple 2-dimensional optimization problem. The Nelder–Mead simplex algorithm [1] is used for the optimization. Figure 2.15 depicts a broadband cancellation result. The system achieves 38 dB cancellation over 60 MHz.

In [17], the delays and attenuations are obtained using tunable lasers with a dispersive element instead of the set of OTDLs and OVAs. This enhances the compactness of the system. Also, a dispersion-induced RF power fading can be easily compensated in this system.

The MPCs above use discrete fiber-optics. The authors in [19] first demonstrated an integrated microwave photonic circuit (IMPC), which requires no fiber. Optical components for the cancellation are monolithically integrated onto a substrate. As the IMPC has no fiber, the cost is significantly reduced. Figure 2.16 illustrates a block diagram and a microscopic image of the IMPC. The IMPC has RF inputs and outputs; it is thus appropriate to be implemented in the RF circuit board. The IMPC achieves 30 dB cancellation over within 400 MHz–6 GHz, which covers all existing FDD LTE and WiFi bands.

2.4.3 Auxiliary Transmit Chain

Suppose that an auxiliary transmit chain generates a copy of the SI signal. This copied SI signal goes through a different channel (\mathbf{h}_{AUX}) from the SI channel (\mathbf{h}_{SI}). The frequency response of the k -th subcarrier of these two different channels are

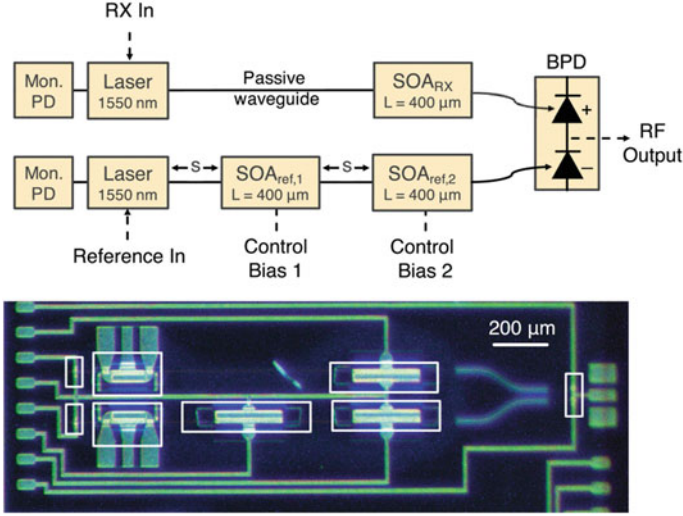


Fig. 2.16 Block diagram and microscope image of the IMPC. © [2017] IEEE. Reprinted, with permission, from ref. [19]

denoted as $(\mathbf{H}_{\text{AUX}}[k])$ and $(\mathbf{H}_{\text{SI}}[k])$, respectively. The basic concept is similar to the adaptive circuit-based cancellation, which generates the copy of the SI signal and subtracts it. First, estimate the two different channels (i.e., $\hat{\mathbf{H}}_{\text{AUX}}$ and $\hat{\mathbf{H}}_{\text{SI}}$). Using the estimated CSI, adjust the input of the auxiliary transmit chain \mathbf{X}_{AUX} as (2.19)

$$\mathbf{X}_{\text{AUX}}[k] = \frac{\hat{\mathbf{H}}_{\text{SI}}[k]}{\hat{\mathbf{H}}_{\text{AUX}}[k]} \mathbf{X}_{\text{SI}}[k], \quad (2.19)$$

where \mathbf{X}_{SI} is the transmitted signal. Note that this method assumes a linear model. Therefore, this method cannot suppress the nonlinear SI components such as transmitter noise.

2.5 Numerical Analysis and Discussions

In this section, we provide a numerical analysis of the SIC methods in an OFDM system. We build a simulator which can analyze the analog–digital integrated SIC performance. For the simulation of analog cancellation, we have to generate the leakages from passive cancellation. Generally, a time-invariant passband channel $h_p(t)$ is represented as

$$h_p(t) = \sum_{i=0}^L h_p^i \delta(t - \tau_i), \quad (2.20)$$

where L is the number of taps, h_p^i is the i -th tap gain, τ_i is the i -th tap delay. Note that the leakage from a circulator consists of three components—direct leakage, reflection from antenna, and reflections from the objects near transceiver.

We assume that the direct leakage has 15 dB attenuation and 300 ps delay, and the reflection from antenna has 17.5 dB attenuation and 3 ns delay. The simulation period is set to 10 ps. A delay of the reflection from the object near transceiver is assumed to be a multiple of 10 ps. Table 2.2 depicts the simulated tap delays and attenuations. A delay line of the adaptive circuit can be modeled as a single tap in $h_p(t)$. In the simulation, we transform $h_p(t)$ to a baseband equivalent form.

Figure 2.17 shows a full-duplex system in the simulation. A simple adaptive circuit is adopted for the active cancellation. The adaptive circuit consist of variable

Table 2.2 Attenuations and delays of the remaining SI after passive cancellation

Source	Attenuation	Delay
Direct leakage	−15 dB	300 ps
Reflection from antenna	−17.5 dB	3 ns
Reflection from objects	−60 dB	20 ns
Reflection from objects	−90 dB	60 ns
Reflection from objects	−100 dB	90 ns
Reflection from objects	−100 dB	120 ns

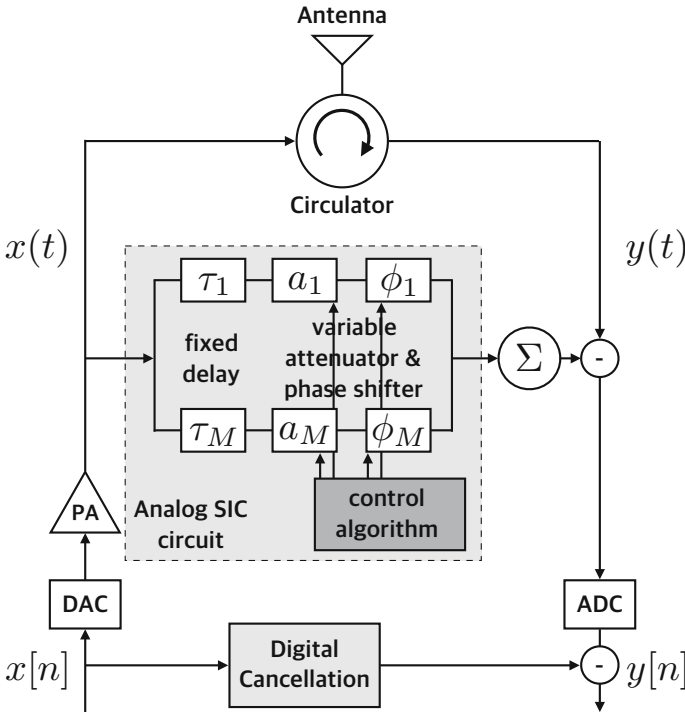


Fig. 2.17 Simulated full-duplex system

Table 2.3 Simulation parameters

System parameter	Notation	Values
Simulation sampling period	T_{sim}	10 ps
Center frequency	f_c	1.5 GHz
Bandwidth	B	20 MHz
FFT size		64
Used subcarrier		52
CP length		16
ADC resolution		14 bit
TX power		-5 dBm
PA gain		15 dB
$P_{1\text{ dB}}$		23.09 dBm
Receiver noise floor		-85 dBm
Adaptive circuit attenuator resolution		∞

attenuators, variable phase shifters, and fixed delays. The fixed delay values are depicted in Table 2.3. The attenuations and phases are set to the solution of the following optimization problem ($\hat{\mathbf{a}}$). Resolution of the variable component is not considered here:

$$\min_{\mathbf{a}} |\mathbf{H}(f) - \mathbf{H}_{\text{cir}}(f)\mathbf{a}|^2 \quad (2.21)$$

$$\text{where } i\text{-th column of } \mathbf{H}_{\text{cir}}(f) = \mathbf{H}_i^{\mathbf{a}_i=1}(f),$$

where $\mathbf{H}_i^{\mathbf{a}_i=1}(f)$ is the frequency response of the i -th fixed delay response with attenuation $\mathbf{a}_i = 1$. As discussed in Sect. 2.2, during the initial stage, the SI signal is transmitted with little power so as to avoid the ADC saturation without the active cancellation.

After the analog cancellation, the residual SI is mitigated by digital cancellation. The greatest obstacle to the digital cancellation is to cancel out the nonlinear SI components, which come mainly from the power amplifier nonlinearity. Several nonlinear digital cancellation methods have been proposed to handle the nonlinearity [8, 9]. A parallel Hammerstein model is widely used to describe the nonlinearity as,

$$x_{\text{PA}}[n] = \sum_{k=0}^{K-1} \sum_{p=0}^{P-1} \psi_{k,p} |x[n-p]|^{2k} x[n-p], \quad (2.22)$$

where $x[n]$ and $x_{\text{PA}}[n]$ are the transmitted and power amplifier output signals on time n , $2K-1$ is the highest order of the model, P is the number of memory taps of the power amplifier, and $\psi_{k,p}$ are the nonlinear coefficients.

Figure 2.18 depicts the power amplifier characteristics which is modeled with the 5-th order parallel Hammerstein (PH) model. In the digital cancellation, we use a simple linear digital cancellation method [15]. The simulation parameters are

Fig. 2.18 Power amplifier characteristics in the simulator (blue line)

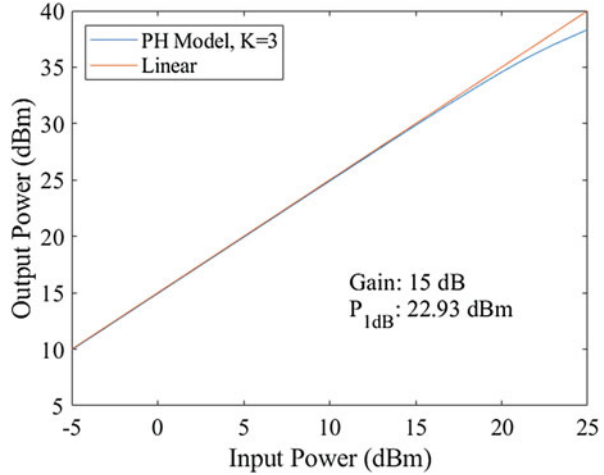


Table 2.4 Analog and digital SIC performance

	10 bit ADC	14 bit ADC
1-tap	Analog cancellation: 44.91 dB	Analog cancellation: 45.36 dB
(1.5 ns)	Digital cancellation: 48.11 dB	Digital cancellation: 48.17 dB
2-tap	Analog cancellation: 48.24 dB	Analog cancellation: 52.76 dB
(0.5 ns, 2.5 ns)	Digital cancellation: 45.13 dB	Digital cancellation: 40.85 dB

presented in Table 2.3. Transmitter noise is not considered here. Analog–digital integrated SIC performance results are depicted in Table 2.4.

The 2-tap adaptive circuit shows a better cancellation performance compared to the 1-tap adaptive circuit. The integrated cancellation amounts are almost the same for the two circuits since the transmitter noise is ignored.

2.6 Conclusion

In this chapter, we introduce an overview of analog cancellation methods in full-duplex radios. First, the necessity of the analog cancellation is explained in the two different aspects: (1) to meet up the ADC dynamic range and (2) to mitigate the nonlinear SI components which cannot be removed in the digital domain (e.g., transmitter noise).

A fact that the power of the transmitter noise in the received SI signal must be lower than the receiver noise floor gives us the insight to design the analog cancellation technique. The transmitter noise is random, therefore, we have only two possible ways to mitigate it: (1) weak the SI signal in a passive manner (passive analog cancellation) and (2) copy the transmitted SI signal and using it as a reference signal to recreate the received SI signal (active analog cancellation, except for

the auxiliary transmit chain method). Various analog cancellation techniques are developed to provide enough cancellation with low complexity (i.e., size of the SI canceller, computational, and power cost) and low bandwidth dependency.

Still, there are some challenges in those issues. Size and power consumption of the adaptive circuit is one of the main bottlenecks to implement the full-duplex in mobile devices. In full-duplex MIMO systems, these practical issues become more severe since the adaptive circuit has to be extended to mitigate both self-talk (i.e., SI) and crosstalk (i.e., interference from the neighbor transmitters).

References

1. J. A. Nelder and R. Mead, "A simplex method for function minimization," *The Computer Journal*, vol. 7, no. 4, pp. 308–313, 1965.
2. C. Cox, *Analog optical links*. Cambridge, U.K: Cambridge Univ.Press, 2004.
3. J. I. Choi, M. Jain, K. Srinivasan, P. Levis, and S. Katti, "Achieving single channel, full duplex wireless communication," in *ACM Mobicom*, Chicago, Illinois, USA, September 2010, pp. 20–24.
4. E. Aryafar, M. A. Khojastepour, K. Sundaresan, S. Rangarajan, and M. Chiang, "MIDU: enabling mimo full duplex," in *ACM Mobicom*, Istanbul, Turkey, August 2012, pp. 22–26.
5. T. Oh, Y. Lim, C. Chae, and Y. Lee, "Dual-polarization slot antenna with high cross-polarization discrimination for indoor small-cell mimo systems," *IEEE Antennas and Wireless Propagation Letters*, vol. 14, pp. 374–377, 2015.
6. M. Chung, M. S. Sim, J. Kim, D. K. Kim, and C. Chae, "Prototyping real-time full duplex radios," *IEEE Communications Magazine*, vol. 53, no. 9, pp. 56–63, 2015.
7. J. G. McMichael and K. E. Kolodziej, "Optimal tuning of analog self-interference cancellers for full-duplex wireless communication," in *Allerton conference on communication, control and computing*, Monticello, IL, USA, October 2012, 2012, pp. 1–5.
8. L. Anttila, D. Korpi, V. Syrjälä, and M. Valkama, "Cancellation of power amplifier induced nonlinear self-interference in full-duplex transceivers," in *Asilomar conference on signals, systems and computers*, Pacific Grove, CA, November 2013, 2013, pp. 3–6.
9. A. Sahai, G. Patel, C. Dick, and A. Sabharwal, "On the impact of phase noise on active cancelation in wireless full-duplex," *IEEE Transactions on Vehicular Technology*, vol. 62, no. 9, pp. 4494–4510, 2013.
10. C. Cox and E. Ackerman, "Demonstration of a single-aperture, full-duplex communication system," in *Radio and wireless symposium (RWS)*, vol. 2013, Austin, TX, USA, January 2013, pp. 20–23.
11. C. Cox and E. Ackerman, "Tiprx: a transmit-isolating photonic receiver," *Journal of Lightwave Technology*, vol. 32, no. 20, pp. 3630–3636, 2014.
12. J. Chang and P. R. Prucnal, "A novel analog photonic method for broadband multipath interference cancellation," *IEEE Microwave and Wireless Components Letters*, vol. 23, no. 7, pp. 377–379, 2013.
13. D. Bharadia, E. McMillin, and S. Katti, "Full duplex radios," pp. 12–16, August 2013.
14. D. Bharadia and S. Katti, "Full duplex mimo radios," in *USENIX symposium on networked systems design and implementation*, Seattle WA, April 2014, 2014, pp. 2–4.
15. J. Kim, M. S. Sim, M. K. Chung, D. K. Kim, and C. Chae, *Signal processing for 5G: algorithms and implementations*. New York, NY, USA, p 539-560: Wiley, 2016.
16. M. P. Chang, C. Lee, B. Wu, and P. R. Prucnal, "Adaptive optical self-interference cancellation using a semiconductor optical amplifier," *IEEE Photonics Technology Letters*, vol. 27, no. 9, pp. 1018–1021, 2016.

17. W. Zhou, P. Xiang, Z. Niu, M. Wang, and S. Pan, "Wideband optical multipath interference cancellation based on a dispersive element," *IEEE Photonics Technology Letters*, vol. 28, no. 8, pp. 849–851, 2016.
18. D. Liu, Y. Shen, S. Shao, Y. Tang, and Y. Gong, "On the analog self-interference cancellation for full-duplex communications with imperfect channel state information," *IEEE Access*, vol. 5, pp. 9277–9290, 2017.
19. M. P. Chang, E. C. Blow, J. J. Sun, M. Z. Lu, and P. R. Prucnal, "Integrated microwave photonic circuit for self-interference cancellation," *IEEE Transactions on Microwave Theory and Techniques*, vol. 65, no. 11, pp. 4493–4501, 2017.
20. E. Everett, A. Sahai, and A. Sabharwal, "Passive self-interference suppression for full-duplex infrastructure nodes," *IEEE Transactions on Wireless Communications*, vol. 13, no. 2, pp. 680–694, 2014.